

# Exploring the assimilation of IASI radiances in forecasting polar lows

Roger Randriamampianina,<sup>a,c\*</sup> Trond Iversen<sup>a</sup> and Andrea Storto<sup>a,b</sup>

<sup>a</sup>*Norwegian Meteorological Institute, Oslo, Norway*

<sup>b</sup>*Euro-Mediterranean Centre for Climate Change, Bologna, Italy*

<sup>c</sup>*Hungarian Meteorological Service, Budapest, Hungary*

\*Correspondence to: R. Randriamampianina, Norwegian Meteorological Institute, Niels Henrik Abels vei 40, PO Box 43, Oslo, NO-0313, Norway. E-mail: rogerr@met.no

We studied the use of IASI data to improve the forecasts of extreme weather events in the Arctic region. For this purpose, the HARMONIE/Norway regional model was used. A set of 366 IASI channels was initially chosen from the ECMWF archived database. Active channels showing the best fit with the analysis system were selected by applying a multi-step monitoring technique. The IASI data were assimilated together with most of the available conventional and operational satellite observations using a three-dimensional variational data assimilation system. Four experiments with cyclic assimilations and subsequent 48-hour forecasts were performed during the IPY-THORPEX campaign period to evaluate the impact of the IASI data and the campaign observations on the hydrostatic HARMONIE/Norway analyses and forecasts.

The assessment of the degrees of freedom for signals on the analysis showed that incorporating the IASI data in the assimilation system improved the contribution of the other observations. The utilization of an energy norm-based approach proved the sensitivity of the forecasts to the IASI channels in cases dominated by dynamic instabilities leading to quickly developing weather systems like, for example, polar lows.

Comparison of the HARMONIE/Norway forecasts against independent observations and the ECMWF analyses showed a clear positive impact of the IASI data on geopotential fields in mid-troposphere and in the troposphere in general, respectively. We found small but significant positive impact on the temperature and humidity in the lower troposphere.

A case-study showed positive impact of IASI radiances on the analysis and forecasts of a polar low. The impact on the forecasts lasted up to 24 hours when extra *in situ* campaign data were excluded from the analysis, and up to 36 hours when the campaign data were assimilated together with the IASI radiances. Copyright © 2011 Royal Meteorological Society

**Key Words:** data assimilation; limited-area model; 3D-Var; satellite observations

*Received 28 September 2010; Revised 18 March 2011; Accepted 5 April 2011; Published online in Wiley Online Library 14 June 2011*

*Citation:* Randriamampianina R, Iversen T, Storto A. 2011. Exploring the assimilation of IASI radiances in forecasting polar lows. *Q. J. R. Meteorol. Soc.* **137**: 1700–1715. DOI:10.1002/qj.838

## 1. Introduction

Providing satisfactory forecasts of fast-developing synoptic systems in areas with a poor conventional observational

network has always been a challenge. This is in particular important for high-impact weather events in the Arctic. Since their appearance, the polar-orbiting satellites have played an important role in observing the polar regions.

These satellites observe a given location twice a day (once during an ascending orbit and once during a descending orbit). Thanks to such a property and to its unique spectral resolution, the Infrared Atmospheric Sounding Interferometer (IASI) instrument (Chalon *et al.*, 2001) is of special interest. IASI is the first infrared interferometer on an operational meteorological polar-orbiting satellite (MetOp). The IASI sensor measures the radiance emitted from the Earth in 8461 channels ensuring a vertical resolution of 1–2 km in the lower troposphere (Collard, 1998; Prunet *et al.*, 1998). Earlier studies (Collard, 1998; Prunet *et al.*, 1998) showed that IASI data contain very useful information for numerical weather prediction (NWP) models. Recently, Collard and McNally (2009) reported significant positive impact of IASI radiances on the European Centre for Medium-range Weather Forecasts (ECMWF) forecasts. Hilton *et al.* (2009) found positive impact of the IASI radiances on the UK Met Office global model forecasts while, for the regional models designed for the short-range forecast, the impact was found to be negligible. However, it was shown at the second International IASI Conference that IASI data provide promising positive impact in the French mesoscale model AROME (Applications of Research to Operations at Mesoscale) (Guidard *et al.*, 2010). Currently, IASI radiances are assimilated in most operational NWP models (Collard *et al.*, 2010).

The Norwegian IPY-THORPEX project (International Polar Year-The Observing system Research and Predictability EXperiment, 2007–2010) aims at significantly improving weather forecasts of severe events, such as polar lows, Arctic fronts, and orographic influences on airflow, through a combined modelling and observational effort (Kristjánsson *et al.*, 2011). The observational effort was based on a 3-week international field campaign out of northern Norway in early 2008, combining airborne and surface-based observations (referred to as campaign observations, Caobs, hereafter). This article deals with the use of IASI observations for improving the forecasts of severe weather events, in particular polar lows (Rasmussen and Turner, 2003), using the HARMONIE/Norway (HIRLAM ALADIN Research on Mesoscale Operational NWP In Euromed) regional model (Randriamampianina and Storto, 2008a). The HARMONIE/Norway model is quasi-hydrostatic and designed for synoptic-scale atmospheric flows. The version of the model used in this study is based on the ALADIN (Aire Limitée Adaptation Dynamique développement InterNational) assimilation and forecast system (e.g. Bubnová *et al.*, 1995; Radnóti, 1995; Horányi *et al.*, 1996; Fischer *et al.*, 2005). Other versions of HARMONIE, using a non-hydrostatic dynamic core, are also developed for operational experimentation at the Norwegian Meteorological Institute (met.no).

Polar lows are very intense maritime storms reaching up to 1000 km in diameter and where the surface winds exceed  $15 \text{ m s}^{-1}$  for part of their existence (Rasmussen and Turner, 2003), and on occasion above  $30 \text{ m s}^{-1}$  (Shapiro *et al.*, 1987). Typically, they last between 12 and 36 hours. Bad forecasts of adverse weather associated with polar lows have cost lives in the past and caused serious damage. There are still occurrences of polar lows that are poorly forecasted and thus may have put human life and property at risk. Polar lows developing in the Norwegian and Barents Seas have therefore been the subject of many studies, including numerical model studies (Grønås *et al.*, 1987) and flight campaigns (Shapiro *et al.*, 1987; Brümmer *et al.*, 2009). Many scientific papers

(e.g. Grønås *et al.*, 1987; Shapiro *et al.*, 1987; Kristjánsson *et al.*, 2011) state that polar lows are triggered by baroclinic instability, but there is also a suggestion saying that release of latent heat by condensation and possibly CISK (Conditional Instability of the Second Kind) plays the primary role for the fast growth and further development of the disturbances (Bratseth, 1985; Emanuel and Rotunno, 1989; Montgomery and Farrell, 1992). A key feature is the relatively high sea-surface temperature experienced when cold Arctic air masses are advected from the ice-covered Arctic Ocean over the open sea. The evidence of the importance of both baroclinic and diabatic processes in the development of polar lows has been also shown through numerical studies (Sardie and Warner, 1983), and in recent ensemble prediction studies (Aspelien *et al.*, 2011; Kristiansen *et al.*, 2011).

In this paper, section 2 describes the HARMONIE assimilation and forecast system. Section 3 presents the particularity of the implementation of the IASI data into the HARMONIE/Norway data assimilation system. Furthermore, in section 4 we assess the impact of the IASI data on the analyses and forecasts of the HARMONIE/Norway regional model through observing system experiments, by evaluating the degrees of freedom for signal related to different types of observation, through estimation of the energy loss in the absence of different observation types in the analysis system and through the discussion of a case-study. Section 5 summarises, and discusses future work.

## 2. The HARMONIE assimilation and forecast system

The HARMONIE/Norway assimilation and forecast system is based on the ALADIN model. It runs in experimental mode at the Norwegian Meteorological Institute. The assimilation system includes a surface Optimal Interpolation scheme to update soil moisture content and skin temperature fields, and an upper-air spectral three-dimensional variational (3D-Var) data assimilation system to analyse wind, temperature, specific humidity and surface pressure fields. Along with all available conventional observations (observations from ground- and sea-based stations (SYNOP); wind profilers (PILOT); radiosondes (TEMP); aircraft reports (AIREP); oceanographic buoys (DRIBU); atmospheric motion vectors (AMV) deduced from the Moderate-resolution Imaging Spectroradiometer (MODIS) aboard TERRA and AQUA), the analysis system comprises the assimilation of microwave radiances from AMSU-A, AMSU-B (Advanced Microwave Sounding Unit) and the Microwave Humidity Sounder (MHS) from the National Oceanic and Atmospheric Administration (NOAA) series and the MetOp polar-orbiting satellites. The microwave radiances are processed at their full resolution in the system according to Randriamampianina (2006). Table I describes the observation usage in our assimilation system. The pre-processing and assimilation of the IASI data are detailed in section 3. No AMV from geostationary satellites are assimilated, due to the domain extension that spans very high latitudes where the scan-angle of geostationary satellites is too far from the zenith path. For the same reason, although the system is able to assimilate the infrared radiances from the Meteosat Second Generation (MSG) Spinning Enhanced Visible and Infrared Imager (SEVIRI), they were not used in this study. Furthermore, Global Positioning System (GPS) zenithal tropospheric delay estimates have not been assimilated in this study, although they are able to

show a positive impact on the forecast skill scores, especially on geopotential and short-range humidity fields (Storto and Randriamampianina, 2010a). The observation operator used for assimilating satellite radiance is the RTTOV (Radiative Transfer for TOVS) radiative transfer model (Matricardi *et al.*, 2004), in its version 8.5. The year-2000 release of the High-resolution Transmission (HITRAN) molecular database (Rothman *et al.*, 1998) was used for generating the database of line-by-line transmittances for fast IASI radiance calculation, with a vertical mesh of 90 levels ranging from 1050 to 0.005 hPa (Matricardi, 2003). Satellite radiances are bias-corrected in accordance with the adaptive scheme of Auligné *et al.* (2007). The background error statistics for the assimilation system were derived by downscaling global ensemble variational assimilation simulations, as described in Storto and Randriamampianina (2010b). The deterministic ECMWF analyses and forecasts were used as lateral boundary conditions. More details about the configuration of the HARMONIE/Norway assimilation system can be found in Randriamampianina and Storto (2008a). The model integration is extended to 48 hours for the midnight and noon runs (0000 and 1200 UTC). The resolution of the model is 11 km in both  $x$ - and  $y$ -directions and the vertical discretization consists of 60 eta levels up to 0.2 hPa. The model domain, using rotated Lambert projection, involves a wide range of latitudes and longitudes. Being centred on Norway, it spans from central Europe to the polar icecap.

### 3. The pre-processing and assimilation of the IASI radiances

#### 3.1. The IASI data (pre-)processing

A set of 366 channels provided by Andrew Collard (Collard and McNally, 2009) was initially used in this study. Three hundred of them are those published in Collard (2007). One field of view (FOV) (always the same) of the four available from each field of regard (FOR) was extracted, guaranteeing that one IASI FOV was chosen for each corresponding AMSU-A FOV. Although there is no dependence between IASI and AMSU-A FOV selection, collocation between the FOVs of these two instruments was chosen to avoid pixel-to-pixel bias variation and better constrain the adaptive bias correction scheme (Collard and McNally, 2009). While some centres are assimilating the IASI radiances without restriction in FOVs (e.g. Météo France: Vincent Guidard, personal communication), similarly to the AMSU-A assimilation, FOVs corresponding to 3 AMSU-A FOVs (FOV with number less than 12 and bigger than 109) on both edges of the satellite track were rejected to avoid larger biases. The active channels were selected by applying a multi-step monitoring technique. Firstly, a set of 93 active channels was chosen after analysing the time series of bias and the standard deviation of the observation departure (observation-minus-first-guess – OMF) and of the analysis increments (observation-minus-analysis – OMA), separately for each channel. The selection was favourable to channels satisfying the applied bias correction scheme (i.e. showing reduction in time within a period of about one month). Then, for the selected channels, the biases attributed to the corrected and non-corrected OMF, as well as the bias attributed to the OMA separately for pixels over land and over sea were analysed (e.g. see Figure 1).

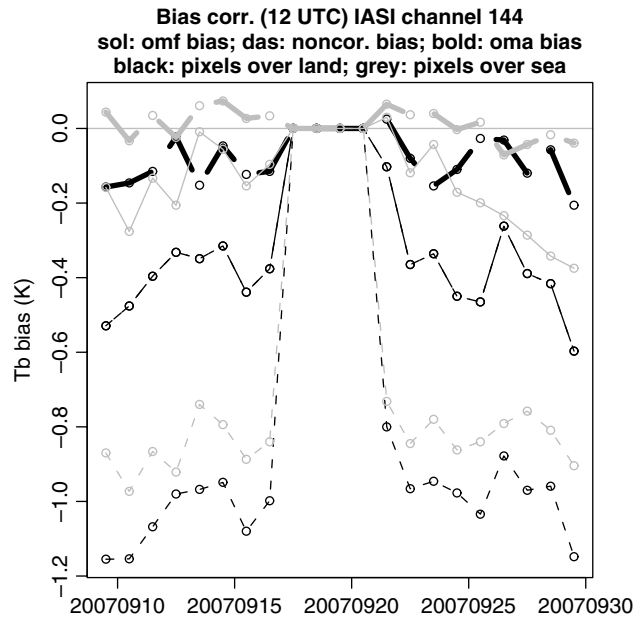


**Figure 1.** Time series for non-corrected (thin dashed lines) and corrected (solid and bold dashed lines) biases. Note that the IASI data were missing for a few days during the test period and that channel 144 peaks around 30 hPa.

The computed statistics for the remained 93 channels have been checked manually one by one, and channels showing clear effective and temporally stable reduction in bias were selected for use. A set of 41 channels, mainly from the CO<sub>2</sub> band, was selected. Note that the relatively small number of active channels was also due to a frequency peak redundancy check, by means of which only one channel was chosen among subgroups of channels peaking closely in the atmosphere. Table II summarises the assimilation of the active IASI channels. Furthermore, for cloudy pixels, active channels having a peak above the cloud top were assimilated. The cloud detection scheme used in this study is a version of McNally and Watts (2003) adapted to the IASI radiances as described in Collard and McNally (2009).

#### 3.2. New strategy for updating the bias correction coefficients for the variational scheme

The radiance bias is the combination of the scan-angle dependent (originating from the measurement quality) and air-mass dependent errors (Eyre, 1992; Harris and Kelly, 2001). For limited-area models (LAMs), it is important to estimate the air-mass bias contribution with the regional model itself instead of using the one estimated by the driving global model that provides the lateral boundary conditions to run the LAM (Randriamampianina, 2005). The default strategy was originally designed for updating the variational bias correction (VarBC) coefficients within global models. It consisted in using, at a given assimilation time, the 6-hour old coefficients estimated during the previous assimilation step. Then, the newly estimated coefficients will be used during the next assimilation process. In the standard formulation of the variational bias correction scheme (Auligné *et al.*, 2007), the bias coefficients (as a function of FOV and air-mass predictors) are minimized within the variational cost function along with the analysis fields. For global models, the coefficients are the averaged values derived from

Table I. The use of observations in the ALADIN-HARMONIE/Norway.

Type	Parameter (Channel)	Bias correction	Thinning
TEMP	U, V, T, Q, Z	Only T, using ECMWF tables	No
SYNOP	Z	No	Temporal and spatial
PILOT ( <i>Europrof.</i> )	U, V	No	Redundancy check against TEMP
DRIBU	Z	No	Temporal and spatial
AIREP	U, V, T	No	25 km horizontal
AMV	U, V	No – Use of quality flags	25 km horizontal
AMSU-A	5 to 13	Variational	80 km horizontal
AMSU-B, MHS	3, 4, 5	Variational	80 km horizontal
IASI	41 channels (see Table II)	Variational	120 km horizontal
GPS-ZTD(*)	ZTD	Air-mass dependent	No
MSG-SEVIRI(*)	5, 6, 7, 9, 10, 11	Variational	60 km horizontal

(\*) Our system is able to use these observations but they were not used in this study.

Table II. The assimilation of the IASI channels.

	IASI_L	IASI_M	IASI_H
Over Sea	193, 207, 214, 217, 219, 222, 224, 226, 228, 230, 232, 236, 299	51, 70, 109, 122, 128, 135, 141, 148, 154, 159, 161, 165, 167, 180, 185, 201, 203, 301	49, 66, 83, 125, 131, 133, 144, 151, 189, 303
Over Land	214, 217, 219	70, 154, 180, 301	133, 303
Over sea Ice	None	None	None

The central wave number of a channel can be determined using the formula  $c = (\text{channel} - 1) \times 0.25 + 645.0$ . IASI\_L, IASI\_M and IASI\_H stand for low-peaking, middle-peaking and high-peaking channels, respectively, according to the definition given in section 4.3.

statistics from both the winter and summer hemispheres over the whole globe. In the case of regional models, depending on the size and position of their domains, at a given assimilation time, we deal with a certain geographical region, in a specific season. Applying the ‘default’ way of updating the VarBC coefficients, for certain satellites at certain assimilation time, it is almost impossible to have the bias reduced in time (Figure 2(a)). This problem of convergence is due to the fact that each satellite senses different portions of the LAM domain at different assimilation times. Hence, different numbers of observations over different atmospheric conditions are taken into account to estimate the bias coefficients for two consecutive analyses. To avoid such an influence, a separate daily update of the coefficients at each assimilation time was adapted (Figure 2(b)). It is also worth mentioning that too small an amount of data at certain assimilation times can be *destructive* (in the sense that the estimated bias is not continuous in time, even with the new technique) in the temporal bias evolution. The optimal use of radiances, with a consistent dataset between different FOVs providing a stable bias at each assimilation time, was reached after blacklisting small and odd paths inside the model domain.

The bias correction coefficients for LAM models are estimated applying a so-called cold-start process. The cold start in bias coefficients estimation is the procedure whereby we start a sequence of data assimilations with zero bias coefficients for radiances computation, so with the real bias of the instrument (Figure 3). Usually, a period of 3 to 4 weeks is enough to get the bias satisfactorily reduced (Figure 3). One can see that a period of roughly one week is enough to considerably reduce the bias from its initial value, when using the new update strategy for the bias correction coefficients.

Figure 4 shows the impact of the new bias correction strategy compared to the ‘default’ one. The impact on the geopotential and temperature (not shown) is significantly positive in the lower troposphere for short-range forecasts.

#### 4. The impact of the IASI data on the HARMONIE analyses and forecasts

The respective impact of the IASI data, assimilated with and without the additional Caobs, is discussed in this section. During the IPY-THORPEX campaign in February–March 2008, additional observations were available in our region of interest, including extra radiosondes and dropsondes released from flight missions targeted to cover Arctic weather events, like for example polar low development. There were also additional aircraft and surface measurements operated during the campaign. See Kristjánsson *et al.* (2011) for more details.

The campaign period lasted from 25 February till 17 March 2008, and our experiments started on 22 February 2008 using the down-scaled ECMWF analysis as initial first guess, thus including a 3-day spin-up period. The coefficients for the VarBC for radiance assimilation were estimated over the period from 1 to 21 February 2008. Thus, the assimilation was repeated without cycling the first guess within this period in order to make the VarBC coefficients converge to their season-specific values.

##### 4.1. The impact of the IASI data on the assimilation system

As an index to study the relative impact of observations in the assimilation system, we use the degrees of freedom for signal (DFS), defined as the derivative of the analysis increments

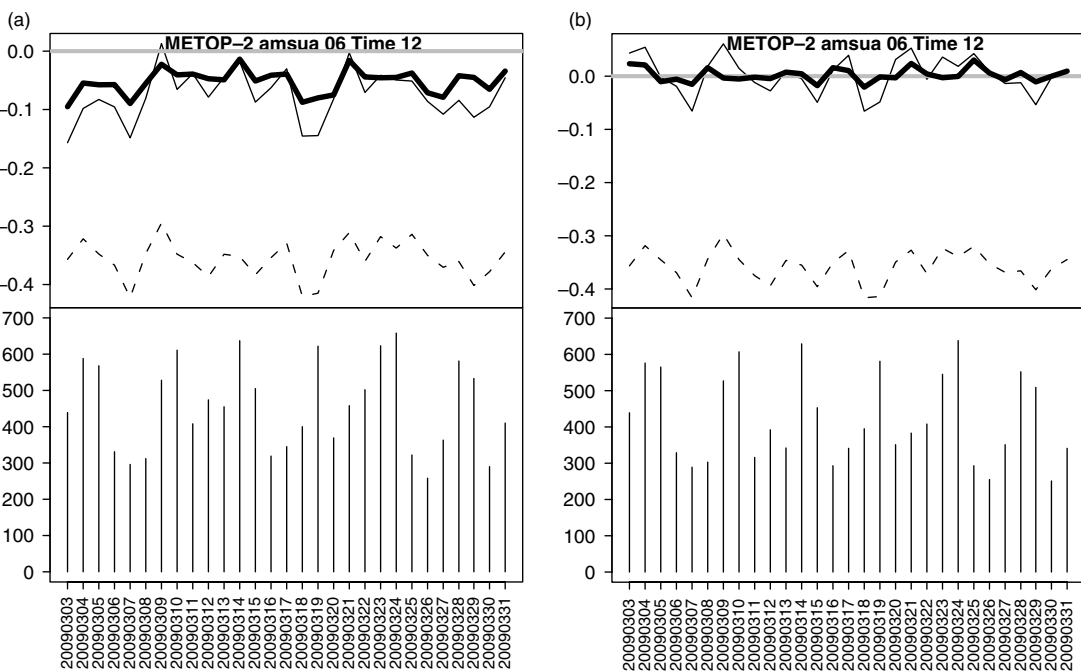


**Figure 2.** Time series of corrected (solid lines) and non-corrected (dashed line) OMF and OMA (bold line) biases (in Kelvin) (upper graphs) for channel 6 of METOP AMSU-A, together with the number of active observations (lower graphs) for the 1200 UTC assimilation time. These graphs show the temporal evolution of the bias by applying the 'default' (a-left) and the new (b-right) update techniques.

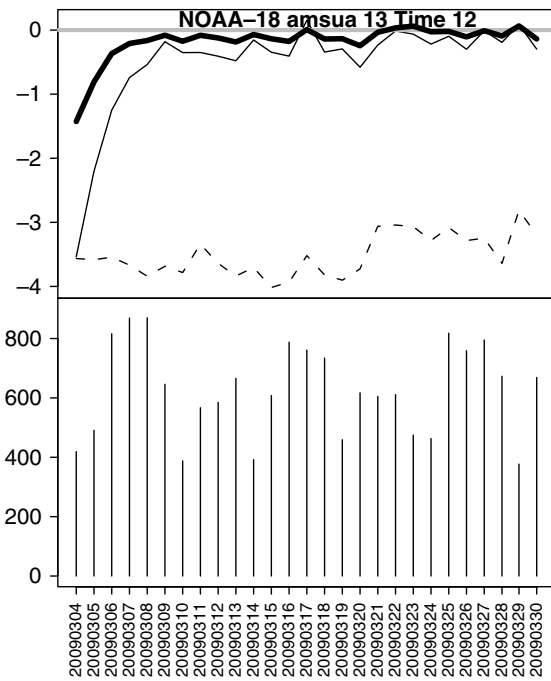


**Figure 3.** The same as Figure 2, but for the case of cold start when applying the new bias correction update strategy, and for channel 13 of NOAA-18 AMSU-A at 1200 UTC assimilation time.

in observation space with respect to the observations used in the analysis system. In practice, it is computed through a randomization technique (Chapnik *et al.*, 2006), which reads:

$$DFS = \frac{\partial(\mathbf{H}\mathbf{x}^a)}{\partial \mathbf{y}} \approx (\tilde{\mathbf{y}} - \mathbf{y})\mathbf{R}^{-1}\{\mathbf{H}(\tilde{\mathbf{x}}^a - \mathbf{x}^b) - \mathbf{H}(\mathbf{x}^a - \mathbf{x}^b)\}, \quad (1)$$

where  $\mathbf{y}$  is the vector of the observations,  $\tilde{\mathbf{y}}$  is the vector of perturbed observations,  $\mathbf{R}$  is the observation-error

covariance matrix,  $\mathbf{H}$  is the tangent-linear observation operator for each observation type,  $\mathbf{x}^a$  and  $\mathbf{x}^b$  are the analysis and the background state, respectively, and  $\tilde{\mathbf{x}}^a$  is the analysis produced with perturbed observations. The previous formulation can be applied to any subset of observations.

The absolute DFS represent the information brought into the analyses by the different observation types, in terms of amount, distribution, instrumental accuracy and observation operator definition. They offer an insight to the actual weight given to the observations within the analysis system in terms of self-sensitivity of the observations (i.e. sensitivity at observation location). However, they do not provide any information on the spatial or cross- correlations between the observations and the analysis. Relative DFS (DFS normalized by the amount of the observations belonging to a specific subset) provide a theoretical value associated with each observation type, regardless of its actual amount and geographical coverage in the analysis system. DFS as a diagnostic tool has been successfully used in different studies. For example, Rabier *et al.* (2002) used it to perform channel selection on simulated IASI radiances, while Cardinali *et al.* (2004) and Montmerle *et al.* (2007) applied it to study the respective influence of different types of observations in an analysis system. For the DFS computation the following times and dates were chosen five days apart to reduce the interdependency between the initial conditions, as recommended in Sadiki and Fischer (2005): 0000 UTC (27 February), 0600 UTC (3 March), 1200 UTC (8 March), and 1800 UTC (13 March).

In Figure 5 the DFS calculated separately for different observation types and parameters are shown. The values represent the sum over the observations belonging to the same subset of Eq. (1) calculated for each individual observation. Analysing the absolute and relative (not shown) values of DFS attributed to different observation types, one can see that adding the IASI data in the analysis system

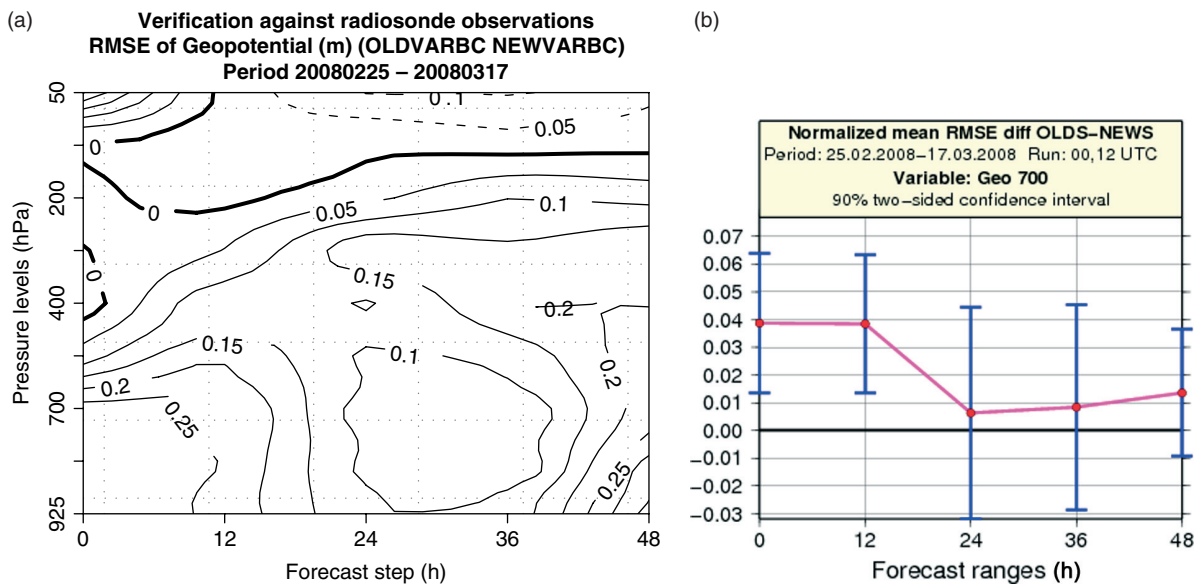


**Figure 4.** The vertical cross-section (left) of the difference between the root-mean-square errors (RMSE) of runs applying the default (old) and the new bias updating strategy evaluated against independent observations. Positive (negative) values correspond to positive (negative) impact. The respective significance test of the impact at 700 hPa model pressure level is shown on the right-hand side. This figure is available in colour online at [wileyonlinelibrary.com/journal/qj](http://wileyonlinelibrary.com/journal/qj)

improves the use of most of the assimilated observations, in the sense that the information brought by the observations increases. In the experiments without the additional Caobs the use of IASI radiances improves the assimilation of AMSU-B/MHS, DRIBU, PILOT, AIREP winds, and TEMP winds and temperature. Furthermore, the assimilation of TEMP humidity, AIREP temperature as well as AMV is also improved in the experiments with the Caobs. Considering Eq. (1), the DFS increase by means of IASI data assimilation is likely to be due to the general improvement of the first guess, i.e. the decrease of the analysis increments. This is also true for the IASI DFS increase when also Caobs are assimilated. Nevertheless, we found that IASI DFS are smaller than for AMSU-A and – B. This seems to be due to the smaller amount of IASI observations with respect to AMSU-A, given the different horizontal spacing used for data thinning. Moreover, AMSU-A is onboard several platforms (NOAA and MetOp satellites) whereas IASI is only onboard the MetOp satellite. Up to 41 channels are used from IASI, with 9 from AMSU-A. Comparing the AMSU-A DFS for the individual satellite we observed an increase of DFS in runs with Caobs for all NOAA satellites (Table III). Further, we observed a reduction in DFS, but with increased number of active observations for MetOp when adding the IASI radiances in the analysis system. For a run without Caobs, only DFS for NOAA-16 has increased when the IASI radiances were added into the assimilation system. We also suspect that IASI observational error variances (2 K for channels 49–193, and 0.5 K for the rest of the active channels) are overestimated. This issue will be subject of further investigation. For the run with Caobs, the overall relative DFS for the assimilated radiances are 0.032, 0.039 and 0.036 for AMSU-A, AMSU-B/MHS and IASI, respectively. Concerning the run without Caobs, the respective relative DFS are 0.031, 0.039 and 0.034.

The magnitude of the OMB and the OMA related to the active channels for the studied case are shown in Figure 6 (see also section 4.4). The magnitude of the OMA with respect to the OMB depends on the statistical properties

of the background and the observation errors. Note that we do not account for the interchannel error correlation in radiances assimilation. For reliable statistics, two days data accumulation (15 and 16 March 2008) was used in the computation. We still observe larger OMA than OMB for some channels, which is probably due to the vertical background error correlation.

#### 4.2. The impact of IASI data on the forecasts

We assessed the impact of the IASI data with and without the additional Caobs through data denial in four experiments. The forecasts initialised at 0000 and 1200 UTC have a maximum range of 48 hours, while those initialised at 0600 and 1800 UTC have a range of 6 hours, only to ensure 6-hour background fields for the next assimilation cycle. The bias and the root-mean-square error (RMSE) of each experiment have been compared against independent observations (surface and radiosonde measurements, using the European Working Group on Limited Area Modeling (EWGLAM) station list (Hall, 1987)) and ECMWF analyses. Significance tests of the objective verification scores were also performed. The significance was examined based on the statistical *t*-test of the difference in the expected values of the RMSE scores of the compared experiments. The graphs are provided together with error bars that represent the interval in which the RMSE difference falls within the 90% confidence level. On the significance test plots, a positive impact is found if the curve lies above the zero line on the vertical axis. The impact is significant if the error bar does not cross the zero line.

We found a clearly positive impact of the IASI data on the geopotential fields, when comparing the RMSE difference between runs with and without IASI data. This is similar to the results published in Hilton *et al.* (2009) and Collard and McNally (2009). Figure 7 demonstrates this impact for the runs without the additional Caobs. The larger error bars on the results related to the comparison against observations come from the relatively small sample in the

Table III. Number of active AMSU-A observations ( $N$ ) and the  $DFS$  for different satellites.

	IASI + Caobs		IASI		Caobs		noIASI	
	$N$	$DFS$	$N$	$DFS$	$N$	$DFS$	$N$	$DFS$
NOAA-15	8770	268.366	8674	258.562	8559	267.443	8609	268.412
NOAA-16	2102	68.915	2083	62.362	2138	64.159	2136	58.577
NOAA-18	21 454	726.439	21601	684.436	21 614	704.429	21 600	712.871
MetOp-2	10 272	317.562	10229	367.54	10 300	319.791	10 244	329.598

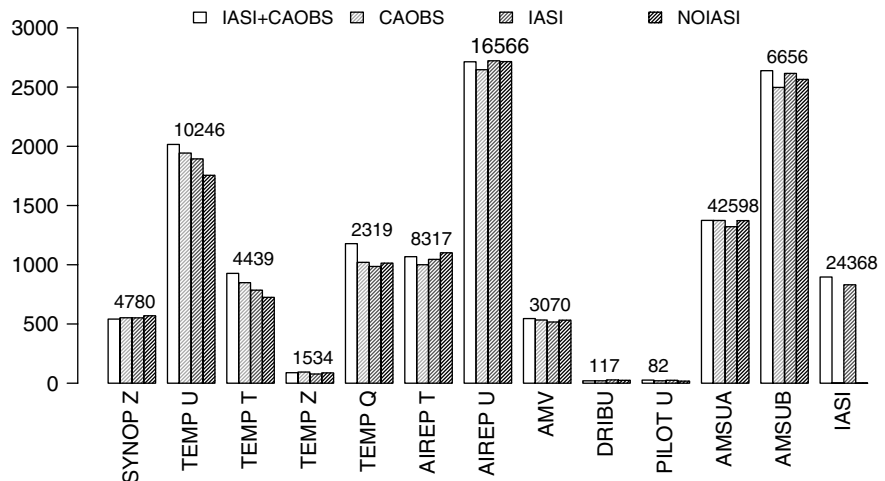


Figure 5. Absolute Degrees of Freedom for Signal grouped by observation types and parameters for all the experiments. The numbers above the histograms refer to the amount of observations for each group relative to the IASI+Caobs experiment.

verification (less than 20 verifying stations against more than 90 000 verifying model grid points for the verification against analyses). We also found smaller but significantly positive impact of IASI data on the temperature and relative humidity in the lower troposphere (not shown). The impact on the wind speed was found rather neutral than slightly positive. The horizontal distribution of the positive impact was found well spread all over the LAM domain (not shown). As expected, the impact is more accentuated over the northern part of the HARMONIE/Norway domain, where we have fewer conventional observations. The *relative impact* of the IASI data on the forecasts is smaller when they were assimilated together with the additional Caobs. The assimilation of the dropsondes, targeted on purpose to sensitive regions, produced much better forecasts. These results confirmed our recent findings on the sensitivity of the HARMONIE/Norway forecasts to the implemented observations, which stressed that the radiosondes are superior to the other observations, especially for the shorter range (1-day) forecasts (Storto and Randriamampianina, 2010c). While the significant positive impact of IASI observations in runs with Caobs lasted up to the 12-hour forecast, it lasted up to 24-hour forecast for the runs without Caobs (Figure 8).

#### 4.3. The sensitivity of the HARMONIE/Norway forecasts to the IASI radiances

A recent technique to assess the impact of different observation types on the forecasts was developed by Storto and Randriamampianina (2010c). The sensitivity of the forecast to the observations is defined by the change in a model

space-based energy norm, between an experiment with all the observations and as many data-denial experiments as the amount of observing networks to which the forecast sensitivity wants to be evaluated. The impact of the observations is evaluated by means of a cost function, given as

$$J = \langle M_t(\mathbf{x}_{\text{ctr}}^a) - M_t(\mathbf{x}_i^a), M_t(\mathbf{x}_{\text{ctr}}^a) - M_t(\mathbf{x}_i^a) \rangle, \quad (2)$$

where  $\mathbf{x}_{\text{ctr}}^a$  and  $\mathbf{x}_i^a$  are the analysis from the ‘all-observations’ experiment and that with the withholding of the  $i$ th observing group, respectively,  $M_t$  is the (fully nonlinear) forecast model operator and  $\langle \dots, \dots \rangle$  stands for the moist total energy norm, defined as in Ehrendorfer *et al.* (1999). Doing this, we are able to obtain an indication of the quality loss associated with the withholding of each observation group or parameter from the assimilation system. We applied this method to evaluate the impact of the IASI data. Based on our earlier experience (Storto and Randriamampianina, 2010c), only the observation types having the largest impact in the assimilation and forecast system were checked together with the IASI data. Such observations are the radiosondes (TEMP), the aircraft observations (AIREP), and the microwave radiances AMSU-A and AMSU-B/MHS. While in the above-mentioned study the sensitivity of the system to each microwave and infrared (from SEVIRI) channel was checked, for sake of simplicity in this study the IASI channels were separated into three groups. According to the vertical distribution of their peaking levels, they were grouped as follows: channels peaking above (IASI\_H, meaning IASI high-peaking channels), around (IASI\_M, meaning IASI middle-peaking channels) and below (IASI\_L, meaning IASI low-peaking channels) 100 hPa (see Table II), considered as a conservative threshold for stratosphere-peaking channels.

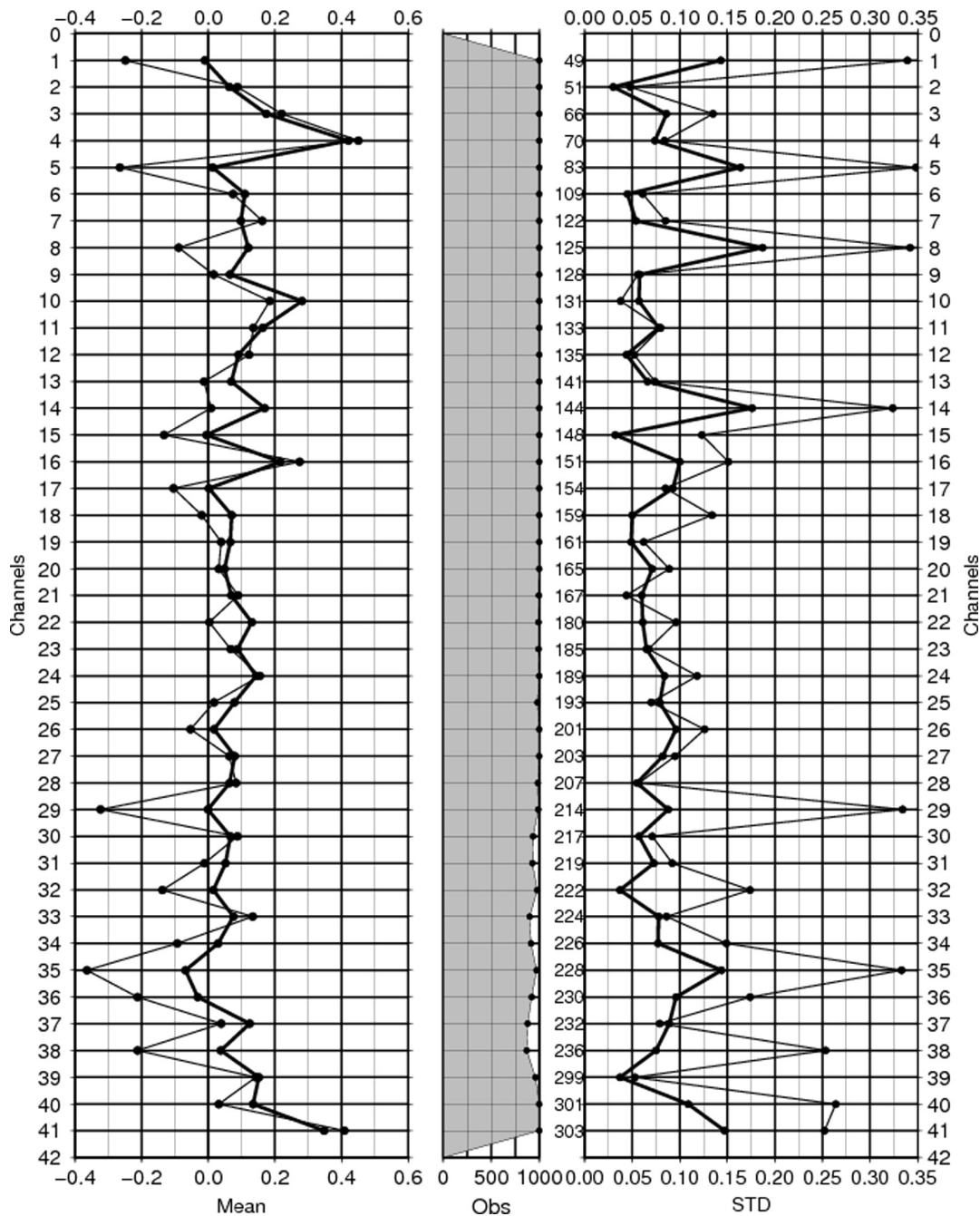


**Figure 6.** The OMF (thin lines) and OMA (bold lines) bias (left) and standard deviation (right), for the experiment with Caobs, for pixels over sea, and estimated for all assimilation times for 15 and 16 March 2008. Left-hand label of the graph on the right represents the channel number in increasing order. The middle graph shows the number of active pixels.

We used for this purpose the experiment with all the observations including all the IASI channel groups along with Caobs. Then, for the overall sensitivity check, data denial experiments should be conducted with predefined dates well distant from each other to ensure independent initial conditions (Sadiki and Fischer, 2005). The scheme is also applicable to check the sensitivity of the forecasts to different observation types relative to specific synoptic conditions or events. Since we are interested in studying the impact of the IASI data in forecasting polar lows, the data denial experiments were arranged for the days with and without polar lows, rather than focusing on the overall impact as described before.

Comparing separately the case-by-case variability of the sensitivity metrics, which represent the relative moist energy norm loss per day, over the cases, we can observe large

variation of the contribution of different observations (Figure 9). One can see that there are cases when the IASI channel groups are able to provide higher impact on the forecasts than the other observations used in the analysis system. These cases include 25 February (1200 UTC), 3 March (0000 and 1200 UTC), 15 March (1200 UTC), and 16 March (0000 UTC) for the 24-hour forecast, for example. Taking into account the synoptic conditions inside the HARMONIE/Norway domain for the investigated cases, we concluded that the radiances, in particular the IASI data, can provide high impact in cases of cloudy and dynamically unstable situations. We analysed the horizontal distribution of the active IASI channels for each investigated case. It seems that for the 0000 UTC analyses, the IASI observations cover only one part of the HARMONIE/Norway domain.

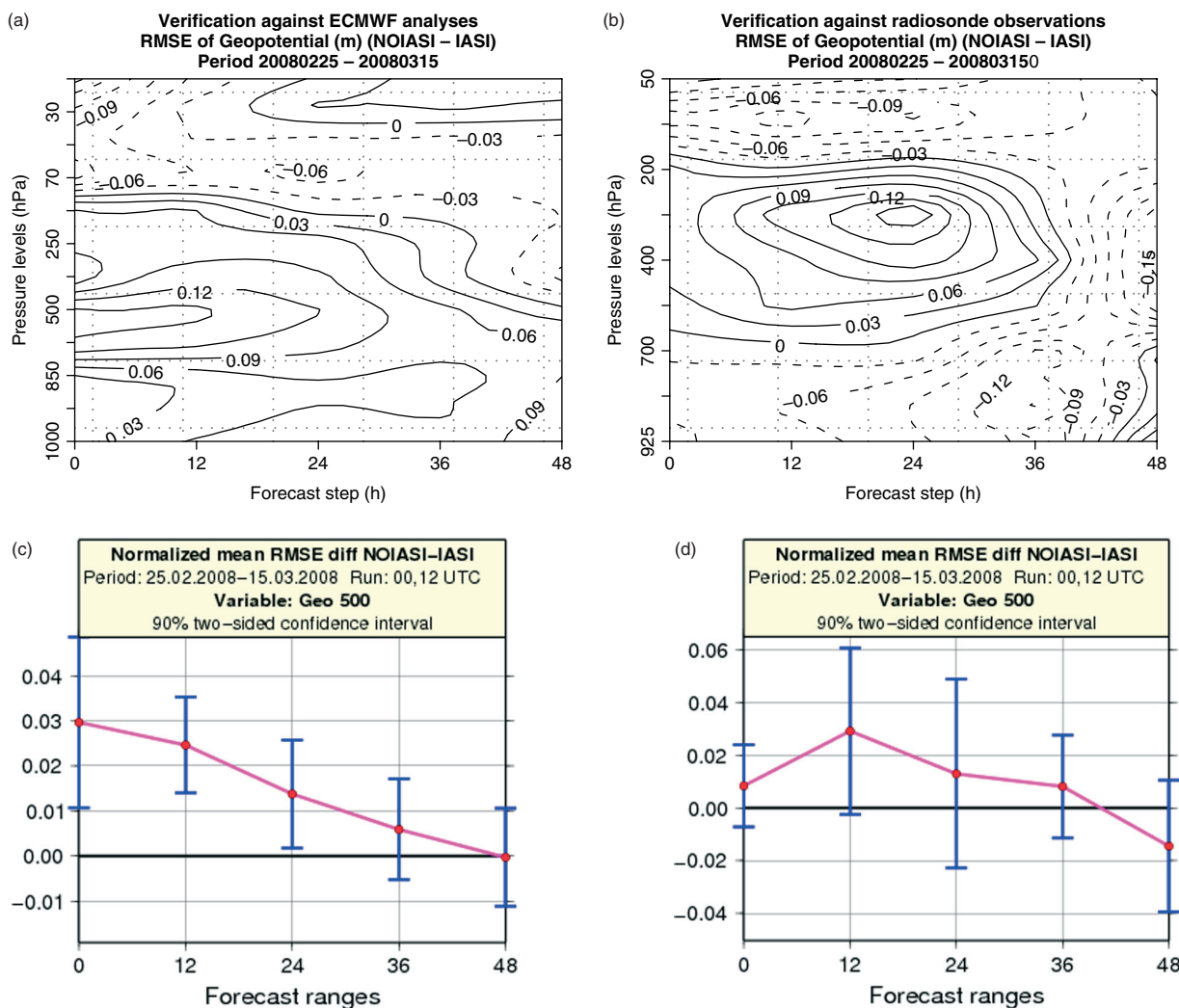


**Figure 7.** Vertical cross-section of the difference between the RMSE of runs with and without IASI data is shown on the top graphs. The comparison against ECMWF analyses and against observations is shown on the left and on the right, respectively. Positive (negative) values mean positive (negative) impact of the IASI data. The corresponding significance test of the impact at 500 hPa model pressure level is given in the lower graphs. This figure is available in colour online at [wileyonlinelibrary.com/journal/qj](http://wileyonlinelibrary.com/journal/qj)

For the case of 3 March (0000 UTC), although a polar low was developing at the northwest of the Lofoten Archipelago, the relatively high contribution from the IASI data was mainly due to the 'perturbations' developing in the southwestern part of the domain. Nevertheless, monitoring the functionality of our data assimilation system (Randriamampianina and Storto, 2008b) we found that, for some cases at 0000 UTC, the IASI radiances can influence the analyses far enough north over the Norwegian Sea, thanks to the properties of our background error statistics. A more interesting situation was observed on 3 March (1200 UTC), when on top of the full observation coverage of the AMSU-A and good coverage of AMSU-B in the southern part of the domain, the IASI data (with good coverage over the domain) had higher relative contribution to the forecasts. Note that the synoptic conditions over the HARMONIE/Norway domain in this case were quite complex. The case of 10 March (1200 UTC) seems to be dominated by a quite 'stationary' synoptic situation over the domain, except for a mature cyclone situated in the southern part of the domain. The case of 15 March, as discussed in section 4.4, was affected by a fast-developing polar low. Also in this case, we can see that the IASI channel groups showed higher energy loss compared to the other radiances assimilated in the system.

Figure 10 shows the horizontal distribution of the active pixels of AMSU-A, AMSU-B/MHS, and IASI radiances on top of the mean-sea-level pressure (MSLP) field. By using RTTOV for generating channel weighting functions for a cloud-free Arctic vertical profile, we found that the lowest peak (around 400 hPa) belongs to channel 219. This suggests that for midlatitude pixels (profiles), this channel would peak higher in the upper troposphere. Taking into account the applied technique for assimilating the IASI channels (section 3.1), and the usual cloud-top height over the Arctic region (e.g. Intriери *et al.*, 2002; Karlsson and Dybbroe, 2010), for this particular day (15 March 2008, 1200 UTC), the channels belonging to the high- and middle-peaking groups were assimilated above the clouds. Regarding the low-peaking channels group, fewer pixels were active for some channels (see also Figure 6) over the southern part of the model domain, presumably due to cloud contamination.

#### 4.4. Case-study

Studying the polar low dynamics, Linders and Sætra (2010) stated that 'Polar lows are a complex weather phenomenon with hotly debated dynamics. There is not even a generally

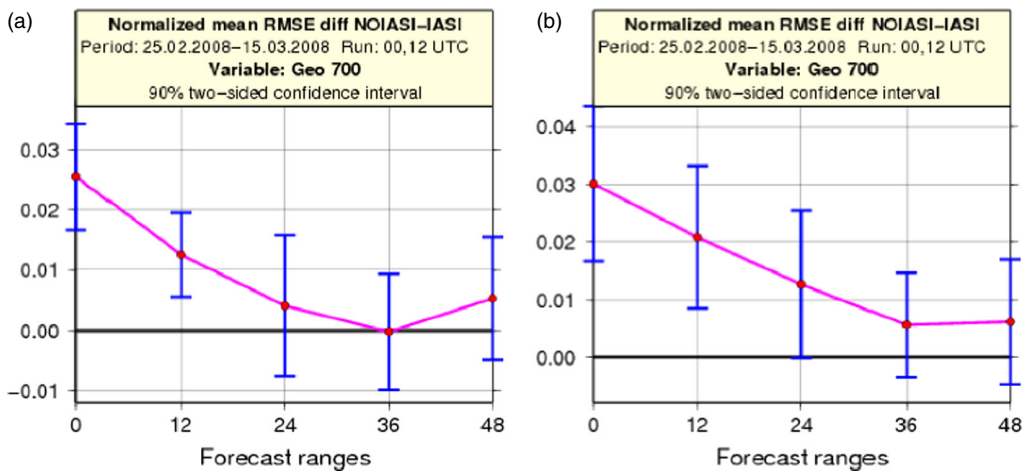


**Figure 8.** Relative impact of the IASI data with (left) and without (right) additional Caobs, expressed in normalized mean RMSE for the 700 hPa geopotential level for verification against the ECMWF analyses. This figure is available in colour online at [wileyonlinelibrary.com/journal/qj](http://wileyonlinelibrary.com/journal/qj)

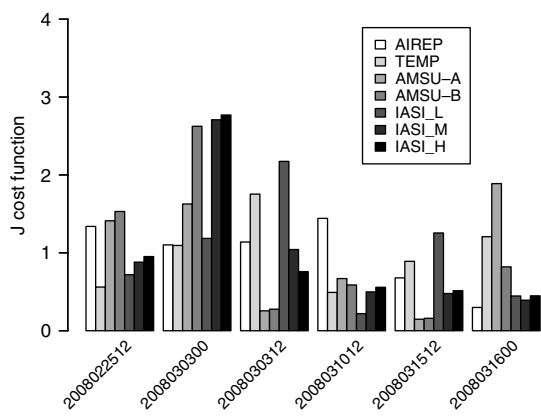


**Figure 9.** Normalised variability of the moist total energy norm over different dates estimated using 24-hour forecasts.

accepted definition . . .'. Although, there is guidance on how the polar lows *are said to develop* (e.g. Shapiro *et al.*, 1987), there are still cases which do not fully agree with them. Nevertheless, the guidance suggests the existence of an upper-level synoptic-scale system together with the polar low developing at the lower levels. We use synoptic charts and cross-sections of wind, relative humidity and equivalent potential temperature (EPT) to identify the polar low and its intensity in our investigation. The wind bars are meant to show the presence of wind shear and wind intensity, while the cross-section of *u*-component (the east–west component) of the wind is meant to check for the presence of near-surface and tropospheric vortices. The cross-section of the equivalent potential temperature is used to check its gradient as a criterion for dynamic instability. Finally, according to the observations (Linders and Sætra, 2010; Kristjánsson *et al.*, 2011), the cross-section of humidity should show dry air at the centre of the low as signature of stratospheric air intrusion.

There were few polar lows developing during the Norwegian IPY-THORPEX campaign period (e.g. Linders and Sætra, 2010; Kristjánsson *et al.*, 2011). We have chosen, as the most interesting one, the case of the polar low, appearing almost at the end of the campaign, whose life cycle roughly lasted from one and a half to two days. This case was observed by dropsondes operated on 16 March from 1100 to 1430 UTC and on 17 March from 0500 to 0830 UTC.

According to our model, the formation of the low started on 16 March at 0000 UTC, and then it reached its mature stage sometimes between 1200 and 1800 UTC, and started its dissipation after roughly one and a half days, when reaching the land, at 1200 UTC on 17 March.

Note that this polar low was not well forecasted by the operational models used in the campaign planning.

In this study we assess the performance of the HARMONIE/Norway regional model in forecasting the position and intensity of this polar low at its culmination and mature stage on 16 March at 1200 UTC. For a subjective verification against the surface measurements, we also discuss the forecast of the polar low at its dissipating stage, situated close to the coast of Norway. Based on the score skills discussed in section 4.2, we use the analyses from the run using the IASI data together with the additional Caobs as the most accurate ones, to illustrate the development of the low (Figure 11). The runs with Caobs (with and without IASI data) analysed the low to be deeper (more than 2 hPa) than the deterministic ECMWF one. But all the analyses fit well with the picture taken by the NOAA-16 satellite at 1150 UTC (not shown).

We have checked different lengths of forecasts valid for the same time: the 12-hour, 24-hour, and 36-hour forecasts for the studied case, and compared the MSLP charts. The 12-hour forecasts were found good enough for predicting the polar low and providing a good warning decision (not shown). But we found clear differences in 36-hour forecast charts, where only the run with all observations included (Caobs and IASI) could provide a reasonable signal (presence of closed isobars) describing the presence of the polar low. Plotting further the cross-sections for the 24-hour forecasts, other interesting differences were found (Figures 12–14). Figure 12 shows the position of the predicted lows and the blue and red cross-section lines. One can see that the runs with the combination of Caobs and IASI (on panels (a), (b), and (c)) provide similar amounts and horizontal extension of the precipitation, but with slightly higher amounts for the run with full observations (panel (a)). The amount of the precipitation associated with the troughs, at their western side, also differs slightly. The run without Caobs and IASI predicts a very specific wave-like perturbation system, with two lows and two troughs. Accordingly, the associated precipitation shows a wave-like extension. The

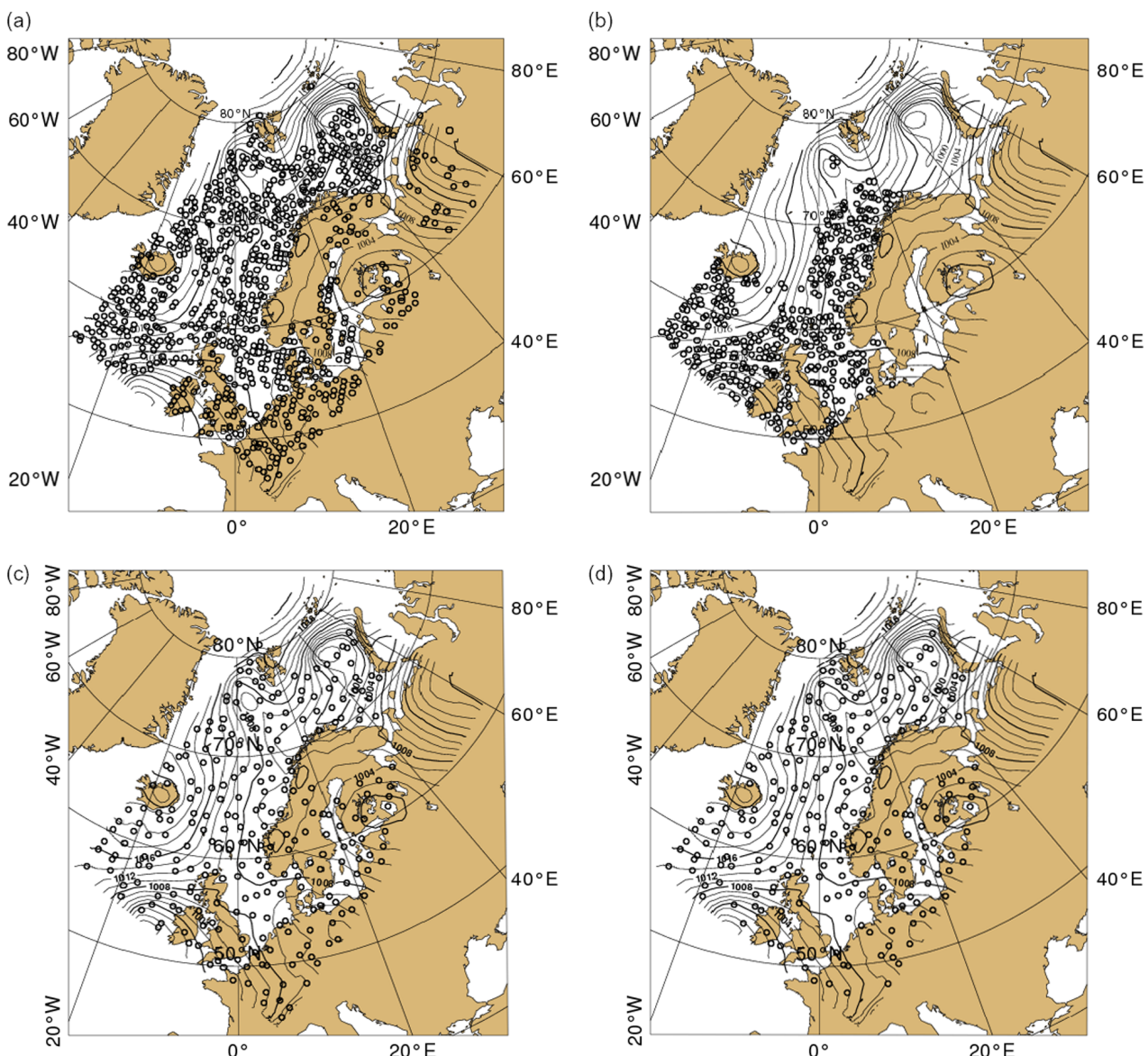


**Figure 10.** The horizontal distribution of (a) the active AMSU-A channel 5, (b) AMSU-B channel 5, (c) IASI channel 154 and (d) IASI channel 219 pixels for 15 March 2008 (1200 UTC), on top of the MSLP field. In this example, channel 154 represents the middle-peaking group, while channel 219 is the lowest-peaking channel within the low-peaking group. This figure is available in colour online at [wileyonlinelibrary.com/journal/qj](http://wileyonlinelibrary.com/journal/qj)

cross-sections through the centre of the low, panels (a), (b) and (c) of Figure 13, show the existence of both the surface and the tropospheric cyclones. Wind barbs on Figure 14 exhibit well the two vortices and the centre of the low where the wind shear exists and the EPT drops (in agreement with Shapiro *et al.* (1987)). On panel (d) of both Figures 13 and 14, where neither the IASI nor the Caobs data were assimilated, the EPT field suggests an extension of instability, which can be a good condition for formation of the wave-like precipitation pattern mentioned above. None of the cyclonic systems are evident on this panel, however. All the panels show the presence of dry air above the centre of the polar low, even in panel (d) above the unstable low-tropospheric layers.

Concerning the 36-hour forecast of the last 6-hour accumulated precipitation, we observed that only one of the four runs could provide similar amounts with similar horizontal extension compared to the results discussed above. Only the run with IASI and Caobs assimilated together could predict a developed low, situated at some

distance from the analysed low, but have a vertical structure satisfying the above-mentioned polar low features (not shown). We notice in this case that the tropospheric cyclone was predicted at lower layers (around 700 hPa) than that predicted in the 24-hour forecast (around 500 hPa).

Figure 15 shows the 30-hour forecasts of the low at its dissipating stage on 17 March at 0600 UTC. The lack of observing network around the forecasted low makes this comparison more complex. But, comparing all the results of the four different runs at once in analysing the intensity of the forecasted low and the pressure associated with the station situated far away from the coast, one can figure out that the low is as deep as about 998 hPa, and the verifying pressure for the mentioned station is close to the 1008 hPa isobar. Based on this assumption, comparing separately the runs with and without Caobs, we can see clearly the impact of the IASI data in forecasting a less deep low (better forecast), while the pressure at the remote station is better forecasted by the runs with Caobs. However, one

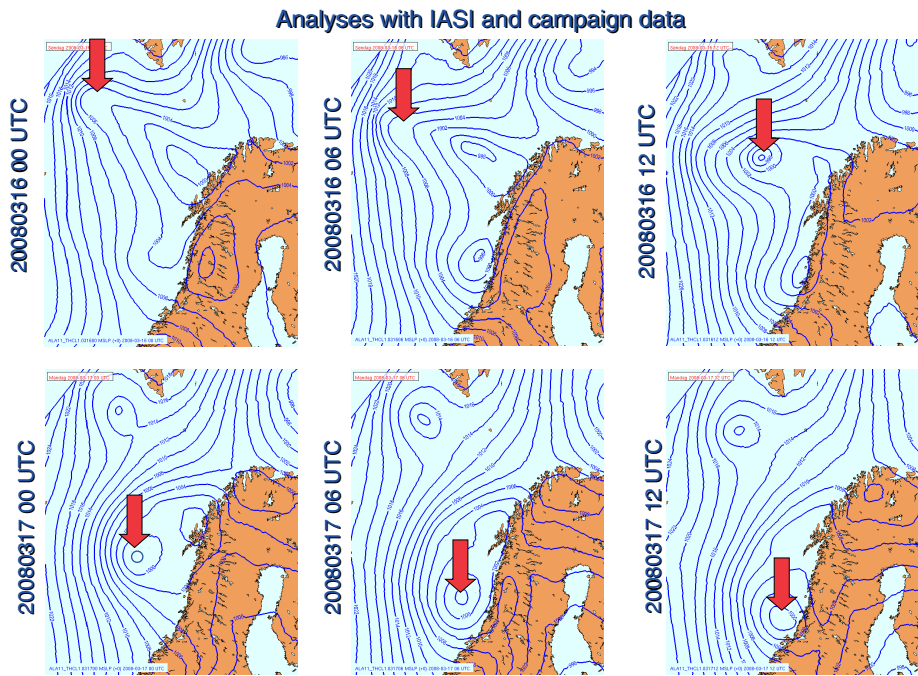


**Figure 11.** The MSLP field analyses of the run with IASI and Caobs at different times. One can see how fast the low was developing. The chart for 1800 UTC is skipped to have the chart with the low reaching land, according the model analyses. The arrows show the positions of the polar low. This figure is available in colour online at [wileyonlinelibrary.com/journal/qj](http://wileyonlinelibrary.com/journal/qj)

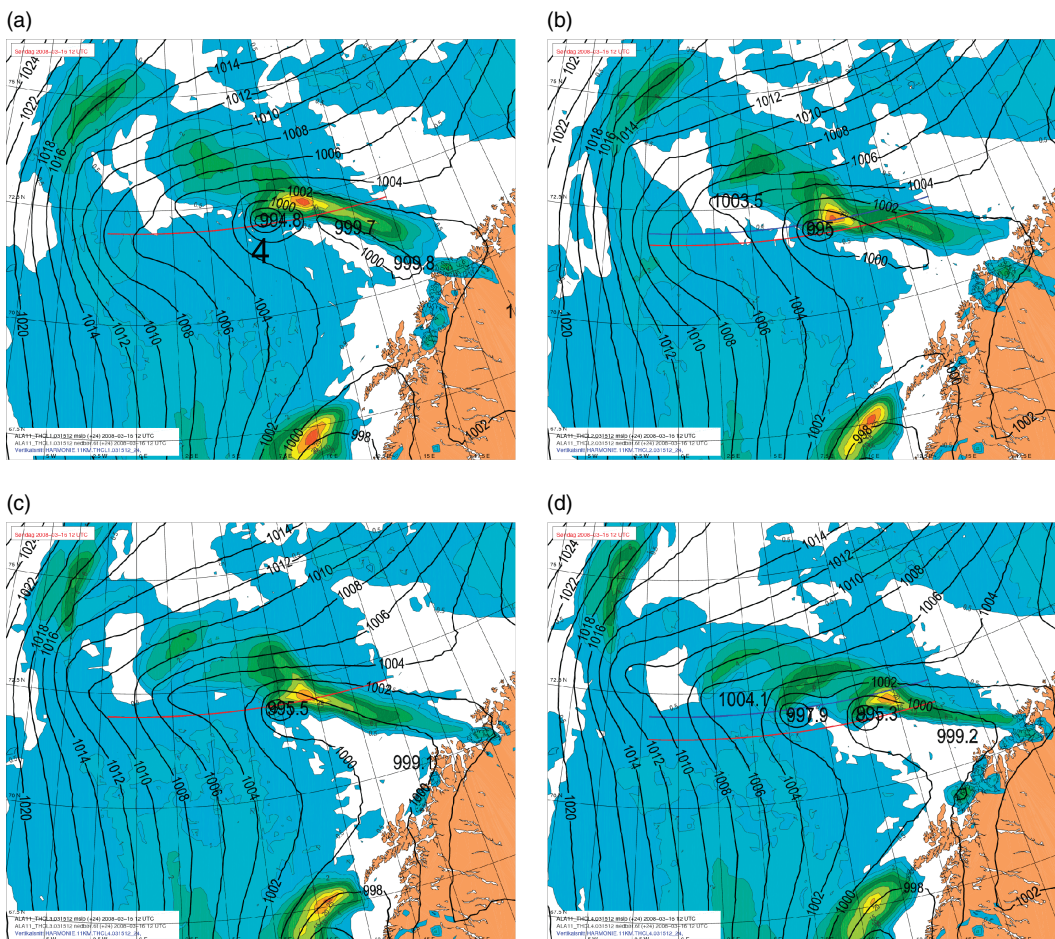


**Figure 12.** The 24-hour forecasts for MSLP and the last 6-hour accumulated precipitation of the run with (left panels) and without (right panels) the assimilation of IASI radiances, and with (upper panels) and without (lower panels) additional Caobs.

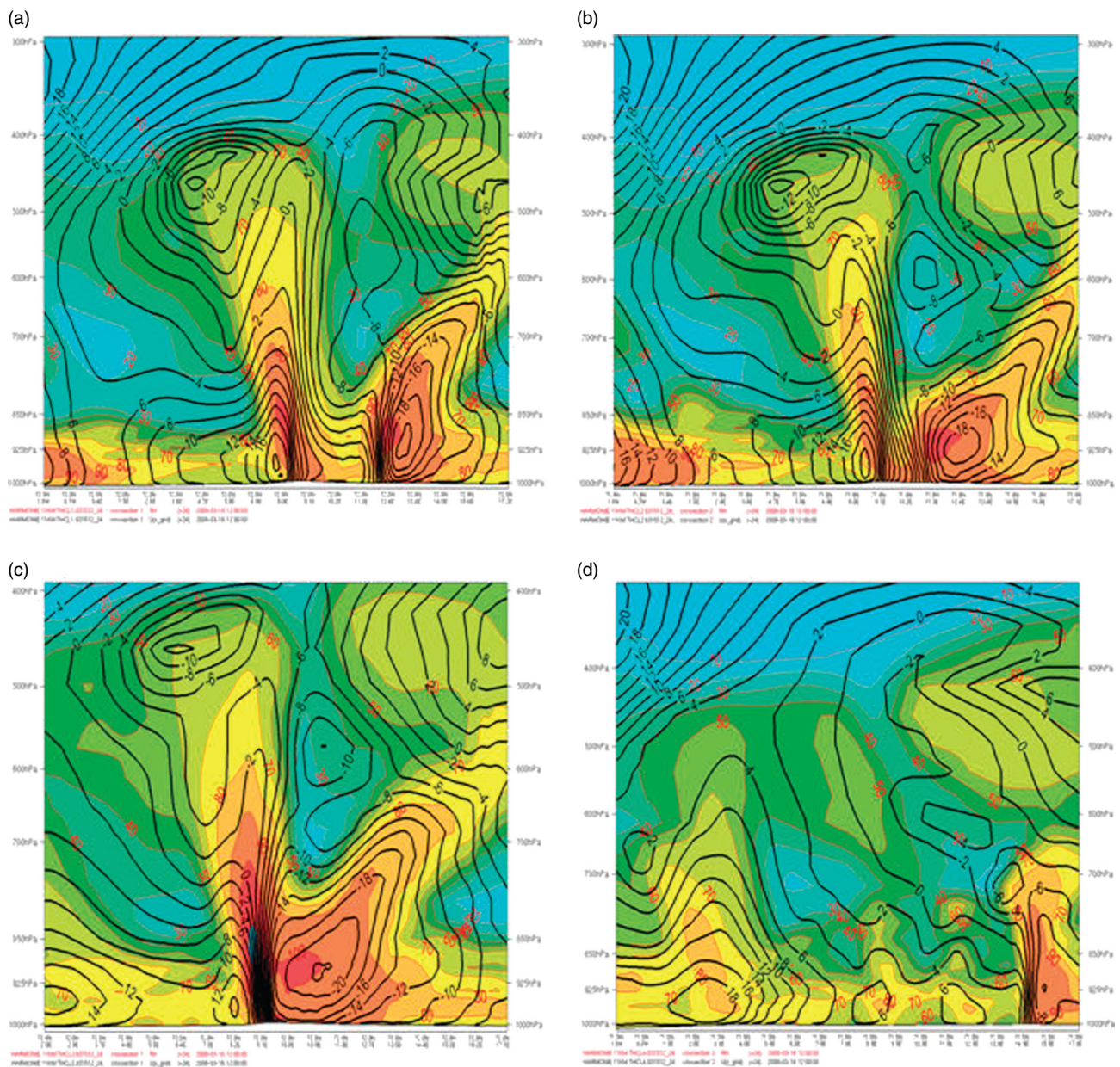


**Figure 13.** The placement of the graphs is the same as in Figure 12. The panels exhibit the cross-section of the wind  $u$ -component (solid lines), and of the relative humidity for the respective 24-hour forecasts. See Figure 12 for the red and blue cross-section lines. Cross-sections (a), (b) and (c) represent zoomed versions along the red lines, but (d) is a zoomed version along the blue line, so for the low located to the west.

can observe larger differences in forecasts of the intensity of the second low or trough (Figures 11 and 15), situated to the north-east of the main low, which imply an overall RMSE for the presented sub-graphs of 2.37 hPa, 2.21 hPa, 2.07 hPa and 1.87 hPa for panels (a), (b), (d) and (c), respectively.

## 5. Summary and discussion

The assimilation of the 41 active IASI channels, mainly from the  $\text{CO}_2$  band, was successfully implemented into the HARMONIE/Norway 3D-Var system. The active channels were chosen by applying a very cautious multi-step monitoring procedure. The optimal usage of the radiance observations was achieved thanks to the new strategy of updating the bias correction coefficients for the VarBC and an additional blacklisting procedure.

A clear positive feedback of the assimilation system with the IASI radiances was demonstrated through a ‘measure’ of absolute value of DFS, when the assimilation of most of the observations in the system was improved.

The impact of the IASI data and the additional campaign observations was assessed through data denial experiments during the Norwegian IPY-THORPEX campaign period. Comparison of the HARMONIE forecasts against independent observations and the ECMWF analyses showed a clear positive impact of the IASI data on geopotential fields in mid-troposphere and in the troposphere in general, respectively. Furthermore, we found small but significant positive impact of the IASI data on the temperature and humidity in the lower troposphere. The impact on wind speed was found rather neutral than slightly positive. Obviously, the experiments with the additional campaign observations were proved to perform better. Consequently, the relative

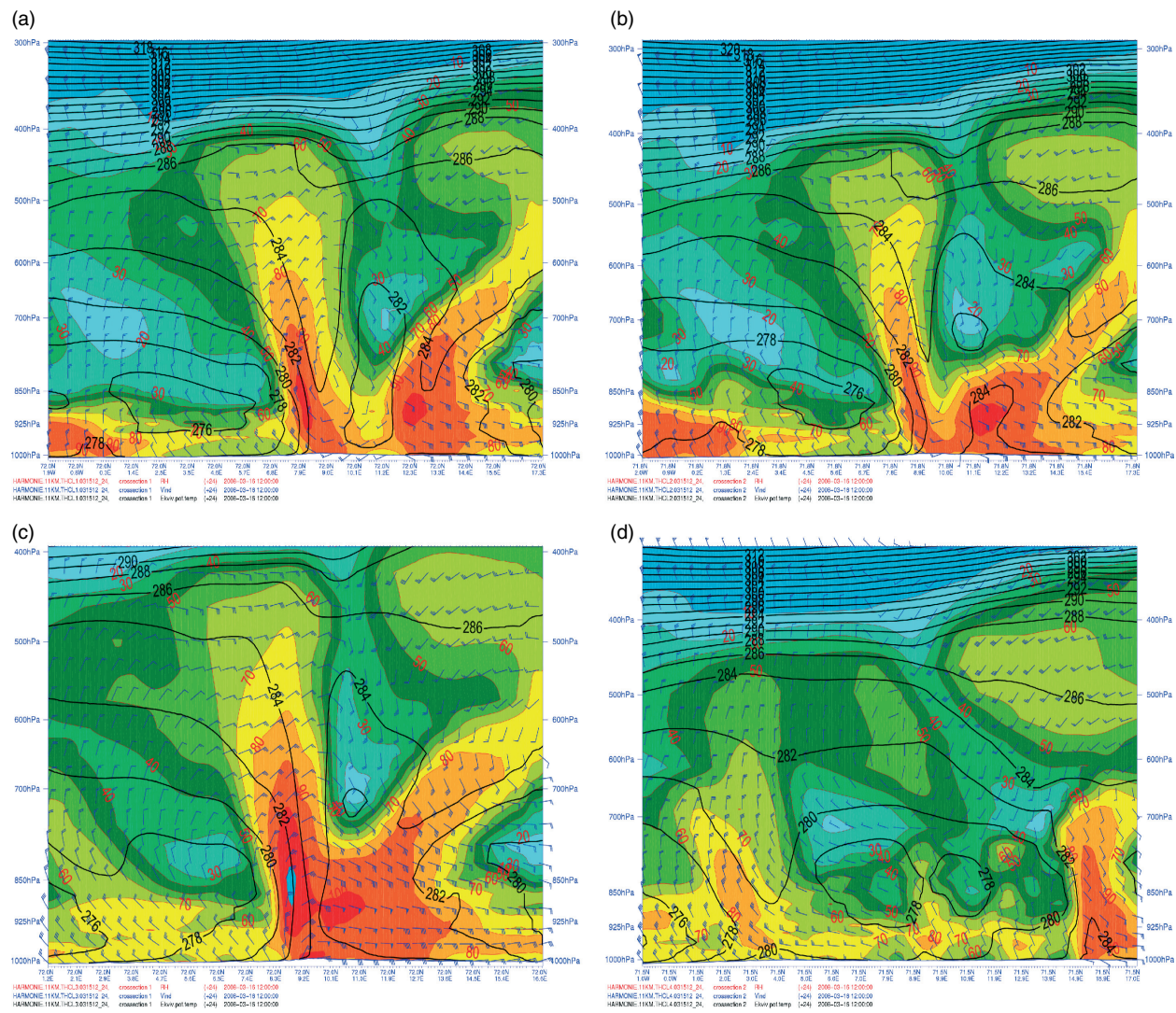


Figure 14. The same as Figure 13, but with the equivalent potential temperature.

impact of the IASI data on the HARMONIE/Norway forecast was smaller in the experiments with than without the campaign observations.

The sensitivity of the HARMONIE/Norway forecasts to the IASI radiances was assessed by evaluating the moist energy loss in the forecast associated with the denial of IASI data in the assimilation system. It was shown that the IASI data can be superior to the other radiances (the advanced microwave data) assimilated in the system, especially in unstable synoptic situations, for example in the presence of a polar low.

A case-study showed that without IASI data in the HARMONIE/Norway assimilation system, the warning of the polar low would be effective only 12 hours ahead. A more-detailed case-study showed that the accuracy of the HARMONIE/Norway forecast system in predicting a polar low development could be improved up to 24-hours by adding the IASI radiances in the assimilation system. Furthermore, this ability of the HARMONIE/Norway model was improved up to 36-hours when the IASI radiances were assimilated together with the additional campaign observations.

Note that during the implementation of the IASI radiances in the assimilation system, the main goal was to have an efficient system rather than the capability of assimilating

as many channels as possible. On top of what was discussed in this paper, the assimilation of radiance data, having an integral property, depends on other things in the system. For example a successful surface assimilation is of interest for the assimilation of low-level peaking and surface-sensitive channels. During the implementation period, we experienced a clear deterioration of the forecast skill scores when low-troposphere peaking channels were assimilated, more probably due to deficiencies in the surface assimilation. Ongoing work is addressing such problems. We believe that it will be possible to add some low-troposphere peaking and even surface-sensitive channels to our data assimilation system soon. Our work on IASI data assimilation, which is one of the Norwegian IPY-THORPEX research engagements, was successful thanks to the ability of the system (IFS/ARPEGE/ALADIN) to assimilate the hyperspectral infrared radiances, such as Atmospheric InfraRed Sounder (AIRS). We will continue our work with adding the AIRS data into our data assimilation system. Note that half of our domain is over sea, where most observations are those measured by satellites, or retrieved from satellite data. We also plan to check whether there are GPS RO (global positioning system radio-occultation) data available inside our domain to support the assimilation of radiances over the remote area and within the stratosphere. This may be

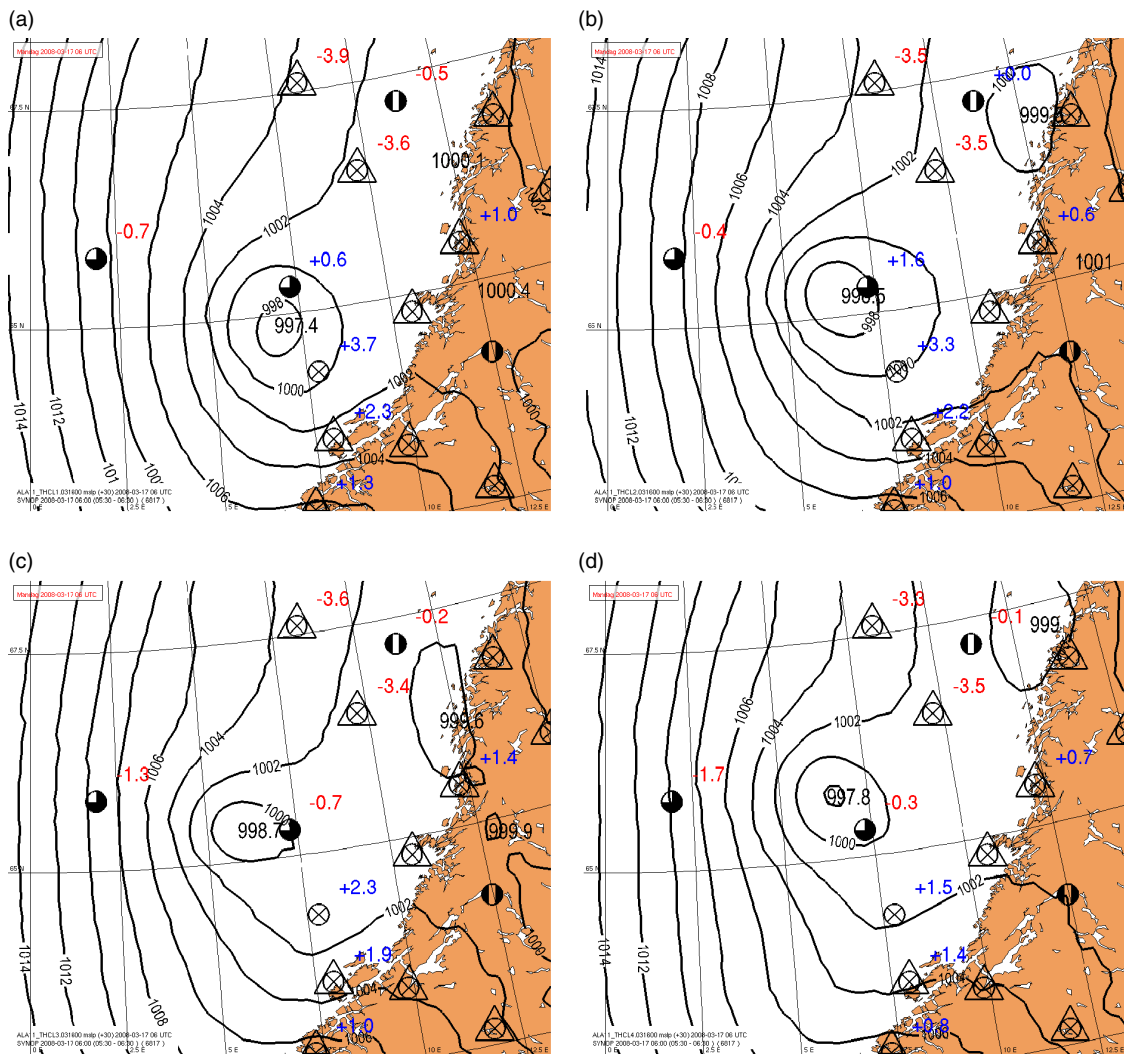


**Figure 15.** The 30-hour forecast of the polar low for the runs with (top panels) and without (bottom panels) Caobs plotted with the difference between observed minus forecasted MSLP. Left panels (a) and (c) show the forecasts with IASI radiances. The MSLP differences are represented as digits next to the surface station (circles) at their upper-right side. This figure is available in colour online at [wileyonlinelibrary.com/journal/qj](http://wileyonlinelibrary.com/journal/qj)

a very important constraint to improve the bias correction scheme in those regions.

#### Acknowledgement

The authors would like to thank the Norwegian Meteorological Institute (met.no), SMHI and Météo-France/GMAP staff for their help, in particular Mariken Homleid, Harald Schyberg, Lars-Anders Breivik, Øyvind Sætra and Nils Gustaffson for fruitful discussion, and Vincent Guidard for his help on observation processing in ALADIN/HARMONIE. The authors acknowledge Fiona Hilton for providing the UK Met Office channel selection information and Andrew Collard for his help in the pre-processing of the IASI channels and in the tuning of the cloud detection scheme. The authors are also thankful to two anonymous reviewers for the help in improving this manuscript. The present study was supported by the Norwegian Research Council through its International Polar Year programme and the project IPY-THORPEX (grant number 175992/S30) – [www.ipy-thorpex.no](http://www.ipy-thorpex.no). The additional dropsonde measurements were operated by the Deutsches Zentrum für Luft- und Raumfahrt (DLR). Computational resources were partly provided by ECMWF through its special project SPNOHARM.

#### References

- Auligné T, McNally AP, Dee DP. 2007. Adaptive bias correction for satellite data in a numerical weather prediction system. *Q. J. R. Meteorol. Soc.* **133**: 631–642.
- Aspelien T, Iversen T, Bremnes JB, Frogner I-L. 2011. Short-range probabilistic forecasts from the Norwegian limited-area EPS: long-term validation and a polar low study. *Tellus* **63A**: 564–584.
- Bratseth AM. 1985. A note on CISK in polar air masses. *Tellus* **37A**: 403–406.
- Brümmer B, Müller G, Noer G. 2009. A polar low pair over the Norwegian Sea. *Mon. Weather Rev.* **137**: 2559–2575.
- Bubnová R, Hello G, Bénard P, Geleyn J-F. 1995. Integration of the fully elastic equations cast in the hydrostatic pressure terrain-following coordinate in the framework of the ARPEGE/Aladin NWP system. *Mon. Weather Rev.* **123**: 515–535.
- Cardinali C, Pezzulli S, Andersson E. 2004. Influence-matrix diagnostic of a data assimilation system. *Q. J. R. Meteorol. Soc.* **130**: 2767–2786.
- Chalon G, Cayla FR, Diebel D. 2001. ‘IASI: An advanced sounder for operational meteorology.’ *Proc. 52nd Congress of IAF, Toulouse, France, 1–5 October 2001*.
- Chapnik B, Desroziers G, Rabier F, Talagrand O. 2006. Diagnosis and tuning of observational error in a quasi-operational data assimilation setting. *Q. J. R. Meteorol. Soc.* **132**: 543–565.
- Collard AD. 1998. ‘Notes on IASI performance.’ Met Office Forecasting Research Technical Report No. 256, 22 pp. Available from the Met Office and at [http://research.metoffice.gov.uk/research/nwp/publications/papers/technical\\_reports/](http://research.metoffice.gov.uk/research/nwp/publications/papers/technical_reports/)
- Collard AD. 2007. Selection of IASI channels for use in numerical weather prediction. *Q. J. R. Meteorol. Soc.* **133**: 1977–1991.

- Collard AD, McNally AP. 2009. The assimilation of Infrared Atmospheric Sounding Interferometer radiances at ECMWF. *Q. J. R. Meteorol. Soc.* **135**: 1044–1058.
- Collard AD, Derber J, Jung J, Hilton F, Pavelin E, Cameron J, Kelly G, Baker N, Ruston B, Garand L, Heilliette S, Guidard V, McNally AP, Eresmaa R, Randriamampianina R, Schwaerz M, Pingel D, Okamoto K, Han W, Le Marshall J, Herdies D. 2010. 'An overview of the assimilation of AIRS and IASI radiances at operational NWP centres.' *17<sup>th</sup> International TOVS Study Conference (ITSC-17), Monterey, California, USA, 14–20 April 2010.* [http://cimss.ssec.wisc.edu/itwg/itsc17/session7/7.9\\_collard.pdf](http://cimss.ssec.wisc.edu/itwg/itsc17/session7/7.9_collard.pdf)
- Ehrendorfer M, Errico RM, Raeder KD. 1999. Singular-vector perturbation growth in a primitive equation model with moist physics. *J. Atmos. Sci.* **56**: 1627–1648.
- Emanuel KA, Rotunno R. 1989. Polar lows as Arctic hurricanes. *Tellus* **41A**: 1–17.
- Eyre JR. 1992. 'A bias correction scheme for simulated TOVS brightness temperatures.' ECMWF Technical Memorandum 186.
- Fischer C, Montmerle T, Berre L, Auger L, Štefánescu SE. 2005. An overview of the variational assimilation in the ALADIN/France numerical weather-prediction system. *Q. J. R. Meteorol. Soc.* **131**: 3477–3492.
- Grønås S, Foss A, Lystad M. 1987. Numerical simulations of polar lows in the Norwegian Sea. *Tellus* **39A**: 334–353.
- Guidard V, Brousseau P, Fourrié N, Rabier F. 2010. 'Impact of IASI assimilation in convective scale model AROME.' *2<sup>nd</sup> International IASI Conference, Annecy, France, 25–29 January 2010.* <http://smsc.cnes.fr/IASI/PDF/conf2/session3/Guidard.pdf>
- Hall C. 1987. 'A common verification scheme for limited area models.' *EWGLAM Newsletter* **15**: 144–147.
- Harris BA, Kelly G. 2001. A satellite radiance-bias correction scheme for data assimilation. *Q. J. R. Meteorol. Soc.* **127**: 1453–1468.
- Hilton F, Atkinson NC, English SJ, Eyre JR. 2009. Assimilation of IASI at the Met Office and assessment of its impact through observing system experiments. *Q. J. R. Meteorol. Soc.* **135**: 495–505.
- Horányi A, Ihász I, Radnóti G. 1996. ARPEGE/ALADIN: A numerical weather prediction model for Central-Europe with the participation of the Hungarian Meteorological Service. *Időjárás* **100**: 277–300.
- Intrieri JM, Shupe MD, Uttal T, McCarty BJ. 2002. An annual cycle of Arctic cloud characteristics observed by radar and lidar at SHEBA. *J. Geophys. Res.* **107**(C10): 8030, DOI: 10.1029/2000JC000423.
- Karlsson K-G, Dybbroe A. 2010. Evaluation of Arctic cloud products from the EUMETSAT Climate Monitoring Satellite Application Facility based on CALIPSO-CALIOP observations. *Atmos. Chem. Phys.* **10**: 1789–1807.
- Kristiansen J, Sørland SL, Iversen T, Bjørge D, Køltzow MØ. 2011. High-resolution ensemble prediction of a polar low development. *Tellus* **63A**: 585–604.
- Kristjánsson JE, Barstad I, Aspelien T, Føre I, Hov Ø, Irvine E, Iversen T, Kolstad E, Nordeng TE, McInnes H, Randriamampianina R, Sætra Ø, Ólafsson H, Shapiro M, Spengler T. 2011. The Norwegian IPY-THORPEX: Polar lows and Arctic fronts during the 2008 Andøya campaign. Submitted to *Bull. Am. Meteorol. Soc.*
- Linders T, Sætra Ø. 2010. Can CAPE maintain polar lows? *J. Atmos. Sci.* **67**: 2559–2571.
- McNally AP, Watts PD. 2003. A cloud detection algorithm for high-spectral-resolution infrared sounders. *Q. J. R. Meteorol. Soc.* **129**: 3411–3423.
- Matricardi M. 2003. 'RTIASI-4, a new version of the ECMWF fast radiative transfer model for the Infrared Atmospheric Sounding Interferometer.' ECMWF Technical Memorandum 425.
- Matricardi M, Chevallier F, Kelly G, Thépaut J-N. 2004. An improved general fast radiative transfer model for the assimilation of radiance observations. *Q. J. R. Meteorol. Soc.* **130**: 153–173.
- Montgomery MT, Farrell BF. 1992. Polar low dynamics. *J. Atmos. Sci.* **49**: 2484–2505.
- Montmerle T, Rabier F, Fischer C. 2007. Relative impact of polar-orbiting and geostationary satellite radiances in the Aladin/France numerical weather prediction system. *Q. J. R. Meteorol. Soc.* **133**: 655–671.
- Prunet P, Thépaut J-N, Cassé V. 1998. The information content of clear sky IASI radiances and their potential for numerical weather prediction. *Q. J. R. Meteorol. Soc.* **124**: 211–241.
- Rabier F, Fourrié N, Chafaï D, Prunet P. 2002. Channel selection methods for Infrared Atmospheric Sounding Interferometer radiances. *Q. J. R. Meteorol. Soc.* **128**: 1011–1027.
- Radnóti G. 1995. Comments on 'A spectral limited-area formulation with time-dependent boundary conditions applied to the shallow-water equations'. *Mon. Weather Rev.* **123**: 3122–3123.
- Randriamampianina R. 2005. Radiance-bias correction for a limited area model. *Időjárás* **109**: 143–155.
- Randriamampianina R. 2006. Impact of high resolution satellite observations in the ALADIN/HU model. *Időjárás* **110**: 329–347.
- Randriamampianina R, Storto A. 2008a. 'ALADIN-HARMONIE/Norway and its assimilation system: The implementation phase.' *HIRLAM Newsletter* **54**: 20–30. Available via <http://www.hirlam.org>
- Randriamampianina R, Storto A. 2008b. 'Monitoring the use of IASI data in a limited area data assimilation system.' *2008 EUMETSAT Meteorological Satellite Conference, Darmstadt, Germany, 8–12 September 2008.* [http://www.eumetsat.int/Home/Main/AboutEUMETSAT/Publications/ConferenceandWorkshopProceedings/2008/SP\\_1232700911980?\\_en](http://www.eumetsat.int/Home/Main/AboutEUMETSAT/Publications/ConferenceandWorkshopProceedings/2008/SP_1232700911980?_en)
- Rasmussen EA, Turner J (eds). 2003. *Polar Lows*. Cambridge University Press.
- Rothman LS, Rinsland CP, Goldman A, Massie ST, Edwards DP, Flaud J-M, Perrin A, Camy-Peyret C, Dana V, Mandin J-Y, Schroeder J, McCann A, Gamache RR, Wattson RB, Yoshino K, Chance KV, Jucks KW, Brown LR, Nemchinov V, Varanasi P. 1998. The HITRAN molecular spectroscopic database and HAWKS (HITRAN Atmospheric Workstation): 1996 edition. *J. Quant. Spectrosc. Radiat. Transfer* **60**: 665–710.
- Sadiki W, Fischer C. 2005. *A posteriori* validation applied to the 3D-VAR Arpège and Aladin data assimilation systems. *Tellus* **57A**: 21–34.
- Sardie JM, Warner TT. 1983. On the mechanism for the development of polar lows. *J. Atmos. Sci.* **40**: 869–881.
- Shapiro MA, Fedor LS, Hampel T. 1987. Research aircraft measurements of a polar low over the Norwegian Sea. *Tellus* **39A**: 272–306.
- Storto A, Randriamampianina R. 2010a. A new bias correction scheme for assimilating GPS zenith tropospheric delay estimates. *Időjárás* **114**: 237–250.
- Storto A, Randriamampianina R. 2010b. Ensemble variational assimilation for the representation of background error covariances in a high-latitude regional model. *J. Geophys. Res.* **115**: D17204, DOI: 10.1029/2009JD013111.
- Storto A, Randriamampianina R. 2010c. The relative impact of meteorological observations in the Norwegian regional model as determined using an energy norm-based approach. *Atmos. Sci. Lett.* **11**: 51–58.